Unsaturated intercellular vapor pressure is relevant for leaf water heavy isotope enrichment

Charlotte Angove[1]*, Marco M. Lehmann[2], Matthias Saurer[2], Yu Tang[3], Petri Kilpeläinen[1,4], Ansgar Kahmen[5], Pauliina P. Schiestl-Aalto[6], Olli-Pekka Tikkasalo[7], Jaana K. Bäck[6] & Katja T. Rinne-Garmston[1]

[1]Stable Isotope Laboratory of Luke (SILL), Natural Resources Institute Finland (Luke), 00790 Helsinki, Finland.

[2]Forest Dynamics, Swiss Federal Institute for Forest, Snow and Landscape Research (WSL), 8903 Birmensdorf, Switzerland.

[3]College of Urban and Environmental Sciences, Peking University, Beijing 100871, China.

[4]Biorefinery and Bioproducts Group, Natural Resources Institute Finland (Luke), 00790 Helsinki, Finland.

[5]Department of Environmental Sciences–Botany, University of Basel, 4056 Basel, Switzerland.

[6]Faculty of Science, Institute for Atmospheric and Earth System Research (INAR)/Physics, University of Helsinki, 00014 Helsinki, Finland.

[7]Carbon Cycle Management Group, Natural Resources Institute Finland (Luke), 00790 Helsinki, Finland.

*__Corresponding email__: charlotte.angove@luke.fi. Telephone: +358 295 322 575

__ORCID IDs__: Charlotte Angove: 0000-0003-2622-2667. Marco M. Lehmann: 0000-0003-2962-3351. Matthias Saurer: 0000-0002-3954-3534. Yu Tang: 0000-0002-2851-4762. Petri Kilpeläinen: 0000-0002-0982-0123. Ansgar Kahmen: 0000-0002-7823-5163. Pauliina P. Schiestl-Aalto: 0000-0003-1369-1923. Olli-Pekka Tikkasalo: 0000-0003-1729-6349. Jaana K. Bäck: 0000-0002-6107-667X. Katja T. Rinne-Garmston: 0000-0001-9793-2549

__Running head__: Vapor pressure effects to leaf water isotopes

Manuscript content notes

Section	Content notes (excludes citations)
Abstract	249
Introduction	1774
Methods	2148
Results	1334
Discussion	1457
Figures	4
Tables (after text)	3
Supplemental Material	Table (1) & Figures (2)

Abstract

Leaf intercellular vapor pressure (e_i) can be unsaturated, but its effect on leaf water heavy isotope enrichment (LWE) has not yet been quantified. We evaluated the ecological relevance of unsaturated e_i for LWE, i.e., for leaf water oxygen-18 and deuterium enrichment, using data from a boreal forest stand and a large-scale dataset. Unsaturated e_i can firstly affect LWE by directly decreasing e_i in the Craig Gordon model (Mechanism 1), which leads to an increased influence of atmospheric vapor isotopic enrichment above source water (Δ_v), and a decreased influence of kinetic fractionation by diffusion through the stomata and boundary layer (ε_k). Unsaturated e_i can secondly affect LWE by changing ε_k (Mechanism 2). To evaluate the effect of Mechanism 1 to LWE, we employed sensitivity tests on LWE model performance using varying measured intercellular relative humidity ($RH_{cellular}$), or $RH_{cellular}$ fitted to observed LWE. To explore the effects of Mechanism 2 to LWE, we modified the calculation of ε_k and observed consequences to LWE predictions. Unsaturated e_i is relevant to LWE by Mechanism 1, since a lowered $RH_{cellular}$ noticeably changed LWE predictions. It clearly improved deuterium predictions and conditionally improved oxygen-18 predictions. Isotope fractionation by Mechanism 2 is unlikely relevant to oxygen-18 and deuterium enrichment. Unsaturated e_i must now be recognized as a variable that introduces error to heavy isotope enrichment models and reconstructions from organic material, via Mechanism 1. We suggest a correction for unsaturated e_i for both oxygen-18 and deuterium enrichment using a variable $RH_{cellular}$ calculated from atmospheric relative humidity.

Introduction

Background

Leaf intercellular spaces are specialized locations for gaseous exchange of CO_2 and water between leaves and the atmosphere. This exchange imprints on the stable isotope signal stored in leaf water, by leaf water heavy isotope enrichment (LWE; Table **1**) (Dongmann *et al.*, 1974; Farquhar *et al.*, 1989; Flanagan and Ehleringer, 1991; Farquhar, Cernusak and Barnes, 2007). Such LWE is merged into the oxygen-18 ($\delta^{18}O$) and deuterium ($\delta^{2}H$) stable isotope values of long-term plant bioindicators (Gessler *et al.*, 2009; Cernusak and Kahmen, 2013; Cueni *et al.*, 2021). For instance, tree-ring $\delta^{18}O$ is a widely applied tool to study environmental variables, such as temperature, precipitation, atmospheric relative humidity (RH_{atm}), and weather phenomena, such as drought (Hartl-Meier *et al.*, 2014; Treydte *et al.*, 2014; Gessler *et al.*, 2018). On the other hand, $\delta^{2}H$ of tree rings might be indicative for carbon metabolic changes (Lehmann *et al.*, 2021; Vitali *et al.*, 2022). Such differences in the behavior of $\delta^{18}O$ and $\delta^{2}H$ are owing to their different molecular masses, different biosynthetic fractionations, and the covariance between RH_{atm} and water vapor $\delta^{18}O$ that is not reciprocated by $\delta^{2}H$ (Cernusak *et al.*, 2022; Holloway-Phillips *et al.*, 2022). Nevertheless, when $\delta^{2}H$ and $\delta^{18}O$ variabilities in tree rings are interpreted using a dual isotope approach, their changes in relative abundance can be used to reconstruct paleoclimatic RH_{atm} (Voelker *et al.*, 2014; Hepp *et al.*, 2017). Leaf water $\delta^{2}H$ is useful for another widely used climatic proxy, leaf *n*-alkanes, which can be used for ecohydrological reconstructions (Sachse *et al.*, 2012).

Despite the many climatic and physiological applications of LWE, recent studies challenge our view on the climate related processes regulating LWE, because LWE predictions assume that leaf intercellular vapor pressure (e_i) is saturated, i.e., that RH inside those pores is 100%, while recent studies show that e_i can be unsaturated, i.e., that RH can drop to as low as 80% (Vesala

et al., 2017; Cernusak *et al.*, 2018; Wong *et al.*, 2022). The effect of unsaturated e_i to LWE is not yet known. If not accounted for, such unsaturated e_i could be a significant source of error to LWE predictions and reconstructions of past climate and plant response to climate change, via interpretation of tree rings and *n*-alkanes.

Currently, LWE is predicted using an adaptation of a model originally used to predict ocean water heavy isotope enrichment, known as the Craig-Gordon model (Craig, 1965; Dongmann *et al.*, 1974; Farquhar *et al.*, 1989; Flanagan and Ehleringer, 1991). An approximate calculation for LWE is:

$$\Delta_e \approx \varepsilon^+ + \varepsilon_k + (\Delta_v - \varepsilon_k)\frac{e_a}{e_i}, \qquad \text{(Equation 1)}$$

where Δ_e is the enrichment of the heavy isotope in leaf water above source water, which is $\Delta^{18}O_{lw}$ for oxygen-18 and $\Delta^{2}H_{lw}$ for deuterium. Source water is often represented by measured or modelled xylem water isotopic value. Then, ε^+ is the equilibrium fractionation factor between liquid water and vapor, and ε_k is the combined kinetic fractionation factor for diffusion of water vapor through the stomata and leaf boundary layer. Next, Δ_v is the isotopic enrichment of atmospheric water vapor compared to source water, e_a is the atmospheric water vapor pressure and e_i is the water vapor pressure in leaf intercellular spaces. Calculations for all variables are demonstrated in supporting information by Cernusak *et al.* (2022). We will hereafter refer to a more accurately assembled version of Equation **1** (Farquhar, Cernusak and Barnes, 2007):

$$\Delta_e = (1 + \varepsilon^+) \times \left[(1 + \varepsilon_k)\left(1 - \frac{e_a}{e_i}\right) + \frac{e_a}{e_i}(1 + \Delta_v)\right] - 1, \qquad \text{(Equation 2)}$$

97 The Craig Gordon model tends to overestimate LWE (Allison, Gat and Leaney, 1985; Leaney
98 *et al.*, 1985; Bariac *et al.*, 1989; Walker *et al.*, 1989). There are three commonly known model
99 corrections to improve LWE model prediction accuracy by considering isotopic
100 inhomogeneities within leaves, and non-steady state conditions. Firstly, the two-pool
101 correction was introduced to reduce LWE overestimation by accounting for the morphological
102 observation that not all leaf water is equally exposed to evaporative enrichment, since most
103 evaporation from leaves occurs at specialized evaporative sites (Leaney *et al.*, 1985; Song *et*
104 *al.*, 2015). Then, the Péclet correction was introduced to correct for back-diffusion of heavier
105 stable isotopologues from evaporative sites (Farquhar and Lloyd, 1993). Finally, non-steady
106 state modelling was introduced for circumstances when transpiration rate is low enough that a
107 relatively slow leaf water turnover rate leads to cumulative LWE (Farquhar, Cernusak and
108 Barnes, 2007). But model corrections do not ubiquitously improve LWE predictions across
109 studies, for example, the Péclet correction is unreliable at improving model accuracy for
110 reasons that are not fully understood, related to the effective path-length (L), which is more
111 like a "fitting parameter" than a measurable dimension (Cernusak and Kahmen, 2013). Other
112 factors known to affect LWE that have not been accounted for in models include xylem water
113 deuterium inaccuracies by cryogenic water extraction artefacts, and xylem sampling effects
114 (Chen *et al.*, 2020; Barbeta *et al.*, 2022; Diao *et al.*, 2022; Nehemy *et al.*, 2022).

115 **Theory for unsaturated e_i effects on LWE**

116 *Mechanism 1*

117 Water vapor pressure is saturated when water vapor is in thermodynamic equilibrium with its
118 condensed state. Originally, there were conflicting views about whether leaf intercellular vapor
119 pressure (e_i) is saturated or unsaturated (Jarvis and Slatyer, 1970; Farquhar and Raschke, 1978;
120 Sharkey *et al.*, 1982; Canny and Huang, 2006). It was only recently, when the first direct

experimental evidence of unsaturated e_i was released (Cernusak *et al.*, 2018; Wong *et al.*, 2022). Unsaturated e_i is particularly relevant to LWE because LWE is caused by the isotopic exchange between leaf water and intercellular vapor. Predictions of LWE rely on an e_i estimate (Equation **2**). When e_i is lowered in Equation **2**, it increases the influence of Δ_v, and decreases the influence of ε_k, to LWE by increasing $\frac{e_a}{e_i}$ (Mechanism 1, Equation **2**). Since very high RH_{atm} (93%) can affect the influence of atmospheric water vapor isotopologues to LWE (Lehmann *et al.*, 2018), an increased influence of Δ_v by decreased intercellular RH ($RH_{cellular}$) is likely relevant to LWE. Similarly, since ε_k is renowned to be important for LWE (Farquhar *et al.*, 1989), a reduced influence of ε_k will likely have a noticeable impact to LWE. Therefore, the effect of unsaturated e_i to LWE by Mechanism 1 is likely impactful to LWE.

If e_i is saturated, it is possible to calculate e_i using only leaf temperature (T_{leaf}; Nobel (2005)). But, since e_i can be unsaturated, there are more factors that contribute to e_i than T_{leaf} (Vesala *et al.*, 2017; Buckley and Sack, 2019). For instance, changes in leaf-atmosphere water fluxes could interact with e_i. Indeed, unsaturated e_i could lead to reduced gross foliar water loss (GFWL), if the equation for transpiration, below, can be used to infer effects of unsaturated e_i:

$$E = \frac{g_s(e_i - e_a)}{p}, \qquad \text{(Equation 3)}$$

where E is transpiration rate, g_s is stomatal conductance, and p is air pressure (Farquhar *et al.*, 1980). But the effects of unsaturated e_i can unlikely be evaluated using Equation **3**, because unsaturated e_i may increase g_s (Buckley and Sack, 2019). Indeed, the water potential (ψ) of intercellular spaces is lowered by unsaturated e_i, which arises many questions about our understanding of leaf water transport biology (Buckley and Sack, 2019). Leaf intercellular spaces might withstand lower ψ by unsaturated e_i, via humidity gradients inside of leaf air spaces that reduce ψ differences between leaf cell walls and intercellular spaces, and by concavely curved water-air interfaces in intercellular spaces (Vesala *et al.*, 2017; Cernusak *et*

al., 2018; Wong *et al.*, 2022). Another consequence of unsaturated e_i is that more water vapor molecules could be up taken from the atmosphere into leaf intercellular spaces, otherwise known as increased gross foliar water uptake (GFWU) which would also depend on RH_{atm} and stomatal conductance (Vesala *et al.*, 2017). Overall, there is no empirical evidence showing that unsaturated e_i would lead to reduced GFWL (Equation **3**) or increased GFWU. Nevertheless, the outcome of both, either reduced GFWL or increased GFWU, contribute to a reduced GFWL:GFWU ratio. The reduced GFWL:GFWU ratio could partly explain the response observed in Equation **2** when e_i is lowered from saturated vapor pressure, which is currently used by literature, to unsaturated vapor pressure.

Mechanism 2

When e_i is unsaturated, it can influence LWE, not only by directly changing e_i in Equation 2 (Mechanism 1), but also by changing the kinetic fractionation factor for diffusion through the stomata and boundary layer (ε_k) used in Equation **2** (Mechanism 2). Unsaturated e_i can change ε_k in two ways. Firstly, it can increase g_s (Buckley & Sack 2019), which affects the calculation of ε_k:

$$\varepsilon_k(H_2{}^{18}O) = \frac{28r+19r_b}{r+r_b}, \quad \text{and} \qquad \text{(Equation 4)}$$

$$\varepsilon_k(HDO) = \frac{25r+17r_b}{r+r_b}, \qquad \text{(Equation 5)}$$

where r is stomatal resistance and r_b is boundary layer resistance (Farquhar *et al.*, 1989). A similar calculation for ε_k has been suggested by Flanagan *et al.* (1991) (Horita, Rozanski and Cohen, 2008). Since r is the inverse of g_s ($r = \frac{1}{g_s}$) (Horita, Rozanski and Cohen, 2008), an increase in g_s decreases r. Such a decrease in r by increased g_s changes ε_k, and could thus affect LWE.

The second way that unsaturated e_i can affect ε_k, is based on the understanding that ε_k represents the nonequilibrium component of leaf water evaporation, where isotope fractionation is controlled by molecular diffusion (Farquhar *et al.*, 1989; Flanagan *et al.*, 1991; Horita, Rozanski and Cohen, 2008). Such nonequilibrium isotope fractionation has recently been adapted to the specialized marine conditions for evaporation from seawater, for example investigating a turbulent component in response to wind speed (Zannoni *et al.*, 2022). Given that ε_k can be adapted for specialized evaporative conditions, ε_k has not yet been adapted for unsaturated e_i. Indeed, if e_i is unsaturated, there would not be ψ equilibrium between apoplastic water and vapor in intercellular spaces, owing to vapor diffusion away from evaporative sites by a small water vapor concentration gradient (Buckley & Sack 2019). Diffusion along a concentration gradient is a source of isotopic fractionation (Merlivat 1978), therefore such diffusion along a concentration gradient within leaf intercellular spaces is a source of isotopic fractionation that could have implications to LWE. Given that Equations **4** & **5** describe kinetic fractionation by stomatal resistance (r) and boundary layer resistance (r_b), we suggest incorporating intercellular resistance (r_i) to account for isotope fractionation by diffusion along a vapor concentration gradient within the leaf intercellular space. We suggest that r_i occurs in Equations **4** & **5** as:

$$\varepsilon_k(H_2{}^{18}O) = \frac{28(r + r_i) + 19r_b}{r + r_i + r_b}, \quad \text{(Equation 6)}$$

and

$$\varepsilon_k(HDO) = \frac{25(r + r_i) + 17r_b}{r + r_i + r_b}, \quad \text{(Equation 7)}$$

respectively. Here, r_i is exposed to the same isotope fractionation (28 & 25) as r, because they are both characterized by diffusive water vapor molecule movement, and they both contribute to a diffusion layer between an equilibrium layer at the air-water interface, and the boundary

190 layer which is characterized by laminar flow. Since Buckley & Sack (2019) calculated that the
191 water vapor concentration gradient in intercellular spaces would be small, it is unlikely that r_i
192 is as influential driving factor to LWE compared to, for example, r. Nevertheless, since it has
193 not been tested before, it is essential to explore whether an introduction of r_i by unsaturated e_i
194 is relevant to LWE.

195 Overall, if e_i is unsaturated, it can have two effects to LWE. Firstly, it increases the influence
196 of Δ_v while decreasing the influence of ε_k (via higher $\frac{e_a}{e_i}$ in Equation 2, Mechanism 1).
197 Secondly, it can affect ε_k by decreasing r and introducing r_i (Equation **6**, **7**, Mechanism 2).
198 Therefore, the main aim of the study was to quantify the effects of unsaturated e_i to LWE model
199 predictions through testing two hypotheses:

200 • Hypothesis 1: Unsaturated e_i increases the influence of Δ_v and decreases the influence
201 of ε_k to an extent that is relevant for LWE, shown by a change in LWE predictions in
202 response to a lower $RH_{cellular}$ (Mechanism 1).
203 • Hypothesis 2: The effect of unsaturated e_i to LWE by changing ε_k, from decreased r and
204 introduced r_i (Mechanism 2), is not influential to LWE compared to other drivers, such
205 as Mechanism 1.

206 There are assets to using *in situ* measurements for evaluating the ecological relevance of
207 violated model assumptions, because there are large quantities of data available, and *in situ*
208 measurements provide an ecological perspective to the relative importance of violated model
209 assumptions compared to other sources of error. We firstly tested hypotheses using survey data
210 on Scots pine (*Pinus sylvestris* L.) in a boreal forest. Since LWE changes between species,
211 seasons, and sites, we also applied our analyses to a large-scale dataset from Cernusak *et al.*
212 (2022) (Snyder *et al.*, 2010; Bögelein, Thomas and Kahmen, 2017; Munksgaard *et al.*, 2017).

Materials and Methods

Field site and sampling

Sampling was conducted at Hyytiälä Forest, which is a managed forest approximately 55 years old, in the southern boreal vegetation zone, southern Finland (61°51'N, 24°17'E, Kolari *et al.* 2022). It is dominated by Scots pine (*Pinus sylvestris* L.), amongst other species, such as Norway spruce (*Picea abies* (L.) H. Karst), birch (*Betula pendula* Roth, *B. pubescens* Ehrh) and European aspen (*Populus tremula* L.) (Kolari *et al.*, 2022). In 2018, the dominant tree height was 23.5m and mean tree height was 19.9m, while tree density was 1304 trees ha^{-1} (Kolari *et al.*, 2022). The soil type is Haplic podzol on glacial till, and in most places soil depth is less than 1m, except for moist depressions, which have a thicker layer of soil with a thin layer of peat above them (Kolari *et al.*, 2022). Precipitation is distributed somewhat evenly throughout the year and mean annual precipitation between 1981 and 2010 was 711mm (Pirinen *et al.*, 2012). Hyytiälä belongs to the Integrated Carbon Observation System (ICOS) network, and a variety of meteorological and leaf gas-exchange parameters are continuously monitored at the site. It is beneficial that there are additional, related tree-physiological investigations from the same site, which can provide deeper insights during data interpretation from this study (Soudant *et al.*, 2016; Leppä *et al.*, 2022; Tang *et al.*, 2022).

Samples were collected between 13:00 and 16:00 during six sampling days with no rain, distributed across the 2019 summer growth season (17 May, 07 June, 28 June, 26 July, 27 August, 23 September). One-year old needles and 2 – 4mm diameter twigs (twig bark was removed) at 18m height were sampled from sun-exposed branches from five Scots pine trees and stored in 12 ml gas-tight glass vials (Exetainer, Labco, UK). All samples were immediately transferred to a cool box. Atmospheric water vapor was collected within the canopy at the same height as needle and twig sampling (18m), on each sampling day, for three hours between 13:00

and 16:00. A dry ice-ethanol cold trap was used, wherein air was pumped into 6mm tubes leading to a U-shaped cold trap (< -70ºC) at 0.7 – 1lmin^{-1}. The U-tube was then immediately capped tightly, removed, then stored in a cool box. Immediately after fieldwork, the collected moisture was transferred into 2ml IRMS vials using a glass Pasteur pipette and stored in a freezer (-20ºC) together with the collected needle and twig samples.

Atmospheric temperature (T_{atm}) and RH (RH_{atm}) were downloaded from the Smart SMEAR AVAA portal (https://smear.avaa.csc.fi/). They were measured onsite, at the ICOS ecosystem station profile, by a Rotronic MP102H RH/T sensor at 16.8m. Leaf transpiration rate was measured using two automated, box-shaped shoot chamber systems made of acrylic plastic (2.1dm^3), surrounding debudded shoots in the uppermost canopy (20m, Aalto et al. (2014)). One cuvette monitored one-year old shoots and a second cuvette measured two-year old shoots, and averages from both cuvettes were used. Cuvettes were ventilated and equipped with a fan. Transpiration rate was calculated by applying a non-linear equation to chamber H_2O vapor concentrations during the first 5 – 35s of intermittent chamber closures (Kolari *et al.*, 2012; Leppä *et al.*, 2022).

Laboratory analysis

Water was cryogenically extracted from needles and twigs at the Swiss Federal Institute for Forest, Snow and Landscape Research (WSL) (West, Patrickson and Ehleringer, 2006). Stable isotope analyses were conducted at The University of Basel Stable Isotope Ecology Laboratory, Switzerland, by Thermal Conversion / Elemental Analyzer (TC/EA) coupled to a Delta V Plus isotope ratio mass spectrometer (IRMS) through a ConFlo IV interface (Thermo Fisher Scientific, Bremen, Germany) (Newberry, Nelson and Kahmen, 2017). Samples were injected at least six times, and a minimum of three of the measurements were used to calculate a mean value, since starting measurements were omitted to compensate for memory effects from the previous sample. Measurements were normalized to Vienna Standard Mean

Ocean Water (VSMOW) using calibrated in-house standards with a δ^2H value of -76.4‰, and a $\delta^{18}O$ value of -10.7‰. Isotope values were defined as:

$$\delta = (R_{sample} - R_{standard})/R_{standard}, \quad \text{(Equation 8)}$$

relative to VSMOW, where R is the D/H or 18O/16O ratio for δ^2H and $\delta^{18}O$, respectively. The standard deviations of quality controls during the time of analyses were 0.3‰ (n = 49) for δ^2H and 0.12‰ (n = 49) for $\delta^{18}O$.

Large-scale dataset sourcing

The large-scale dataset and its LWE predictions were first sourced from the review published by Cernusak *et al.* (2022). This large-scale dataset comprises of 546 datapoints for paired Δ^2H_{lw} and $\Delta^{18}O_{lw}$. The geographical range extends across more than 100º of latitude and there is an elevation range larger than 3000m. Most of the data is from temperate forests or woodlands, followed by tropical forests or woodlands. The data from Hyytiälä was added to the large-scale dataset and, after a grassland in Greenland, it contributed the highest-latitude data and the only boreal forest measurements. The large-scale dataset was filtered to select sampling sites with at least five different sampling times, to meet statistical analysis criteria. Data from Kahmen et al. (2011) were clustered into five main sampling sites, and three sites from Munksgaard et al. (2017) were clustered into one site (Herberton, Wild River & Mount Garnet), so that data met the filter criterion and thus could be included. The resultant dataset constituted of 534 datapoints from Cernusak *et al.* (2022) and 29 datapoints from this Hyytiälä ($\sum$ = 563).

Leaf water heavy isotope enrichment modelling

All modelling and statistical analyses were performed in R (R Core Team, 2022). Observed leaf water and water vapor enrichments were calculated as:

$$(\delta_e - \delta_{source})/(1 + \delta_{source}/1000), \quad \text{(Equation 9)}$$

where δ_e is the isotope value of the parameter whose enrichment above source water is being estimated, i.e., leaf water or water vapor (Cernusak *et al.*, 2016). Firstly, LWE was modelled using Equation **2**, using the calculations provided in the supporting materials by Cernusak *et al.* (2022), for both Hyytiälä and the large-scale dataset. At Hyytiälä, T_{leaf} was first assumed to be the same as T_{atm}, which is a reasonable assumption because the Scots pine needles are small and well-coupled to the atmosphere (Launiainen *et al.*, 2016; Kim *et al.*, 2018; Leppä *et al.*, 2022). Nevertheless, given that there are uncertainties relating to the assumption that T_{leaf} is equal to T_{atm}, and that recent evidence shows that the relationship between T_{leaf} and T_{atm} can change on a diurnal basis (Still *et al.*, 2022), we expanded analyses to include sensitivity of results to a T_{leaf} change of ±2ºC from T_{atm}, to guide inferences on the relative influence of unsaturated e_i to LWE compared to a ±2ºC change in T_{leaf}.

Main results were inferred from the foundational CG model (Equation **2**). A two-pool correction and a Péclet correction were additionally applied, as an initial demonstration of how such corrections can interact with unsaturated e_i. The two-pool correction was calculated as:

$$\Delta_L = (1 - \varphi)\Delta_e, \quad \text{(Equation 10)}$$

where Δ_L is the final calculated leaf water heavy isotope enrichment (LWE), Δ_e is the modelled LWE by the Craig-Gordon model, and φ is the proportion of unenriched xylem water in leaf water (Leaney *et al.*, 1985; Song *et al.*, 2015). The estimate for φ was 0.316, based on Scots pine leaf anatomical measurements by Roden et al. (2015). For the Péclet correction, the Péclet number was calculated as:

$$\wp = \frac{LE}{CD}, \quad \text{(Equation 11)}$$

where L is effective path length, E is transpiration rate (mol m^{-2} s^{-1}), C is the molar concentration of water (5.5×10^{-4} mol m^{-3}) and D is the diffusivity of the water isotopologue responsible for enrichment. Their calculation is described in further detail by Cernusak *et al.*

(2016), and in this study, L was calculated for each sampling date based on transpiration rate. The Péclet correction is applied as P:

$$P = \left(\frac{1-e^{\wp}}{\wp}\right), \quad \text{(Equation 12)}$$

where:

$$\Delta_L = \Delta_e \times P. \quad \text{(Equation 13)}$$

There was limited transpiration rate and φ data availability for the large-scale dataset, so this additional model correction demonstration was only performed for Hyytiälä data.

To explore the effects of unsaturated e_i to LWE by increasing influence of Δ_v and decreasing influence of ε_k (Hypothesis 1), Equation **2** was applied with different assumptions for $RH_{cellular}$ when calculating e_i. For example, in Equation **2**, atmospheric vapor pressure (e_a) can be expressed as:

$$e_a = \text{psat} \times (RH_{atm}/100), \quad \text{(Equation 14)}$$

where psat is saturated vapor pressure. Since e_i was assumed to be saturated during LWE modelling, it has been estimated as e_i = psat. In this study, we calculated e_i in the same way that e_a has been expressed, in Equation **14**, by replacing RH_{atm} with $RH_{cellular}$:

$$e_i = \text{psat} \times (RH_{cellular}/100), \quad \text{(Equation 15)}$$

using the following assumptions for $RH_{cellular}$:

1. $RH_{cellular}$ = 100%. *Saturated* e_i.
2. $RH_{cellular}$ = 90%. *Within the observed range reported by literature (Cernusak et al., 2018; Wong et al., 2022).*
3. $RH_{cellular}$ = 80%. *The lowest approximate* $RH_{cellular}$ *reported by literature (Cernusak et al., 2018; Wong et al., 2022).*

Finally, since RH_{atm} potentially affects $RH_{cellular}$ (Vesala *et al.*, 2017; Cernusak *et al.*, 2018), we modelled $RH_{cellular}$ as a response to RH_{atm}. This was a model-optimization, which used measured LWE to find a fitted e_i along an RH_{atm} gradient for both Δ^2H_{lw} and $\Delta^{18}O_{lw}$. We used:

$$e_i = 0.65 + \frac{0.35}{(1+A \times e^{-B \times RH_{atm}})^{\frac{1}{C}}} \quad . \qquad \text{(Equation 16)}$$

Calculants A, B and C were solved simultaneously for both Δ^2H_{lw} and $\Delta^{18}O_{lw}$, to find one fitted $RH_{cellular}$ for both elements using the optim function in the 'stats' package. The optim function was run with default configuration using the Nelder-Mead algorithm. Fitted $RH_{cellular}$ was also solved for each of Δ^2H_{lw} and $\Delta^{18}O_{lw}$ separately.

When calculating psat for e_a, T_{atm} is used, meanwhile, when calculating psat for e_i, T_{leaf} is used (Cernusak *et al.*, 2016). In Equation **2**, e_i occurs twice, and main results are given for adjustment of both e_i occurrences. An additional post-hoc analysis was performed on data from Hyytiälä, where each occurrence of e_i was adjusted to different $RH_{cellular}$ assumptions, separately.

To test the effect of unsaturated e_i to isotope fractionation associated with r_i, we calculated ε_k using Equations **6** & **7** and implemented the altered ε_k to Equation **2**, to look for observable changes in predicted LWE compared to modelled LWE using ε_k that had been calculated using Equations **4** & **5**. For this, we used data from Hyytiälä when $RH_{cellular}$ was 90% or 80%, and we applied leaf anatomical measurements of Scots Pine needles by Roden et al. (2015). Intercellular resistance (r_i) was estimated using three calculation steps. First, the rate of water vapor diffusion along a concentration gradient within an intercellular space (J, mol m^{-2} s^{-1}) was estimated using Fick's law of diffusion:

$$J = \frac{DA[c_1 - c_2]}{T}, \qquad \text{(Equation 17)}$$

where D is the diffusion constant, at 2.44×10^{-5} m^{-2} s^{-1} (Merlivat 1978), A is the cross-sectional area of diffusion, which we approximated by using cross-sectional leaf area exposed to evaporation per square meter using Scots Pine measurements by Roden *et al.* (2015) (A = 1 - φ = 0.684). Then, c_1 was the concentration of water vapor in the equilibrium layer at the air-water interface in the leaf intercellular space (mol m^{-3}), calculated as saturated vapor concentration at leaf temperature, and c_2 was the unsaturated concentration of water vapor in the unsaturated portion of the leaf intercellular space ($c_2 = c_1 \times (RH_{cellular}/100)$). Such definitions of c_1 and c_2 were based on the principle that there is an equilibrium layer at the air-water interface during evaporation, and because there are humidity gradients inside of leaf intercellular spaces (Wong *et al.* 2022), but they can be improved if more knowledge arises about leaf intercellular space humidity conditions. Finally, T was the length of the diffusion pathway, which has not yet been quantified, we approximated T by using measured mean mesophyll thickness for Scots Pine by Roden *et al.* (2015) (1.71×10^{-4} m).

Intercellular conductance (g_i, mol m^{-2} s^{-1}) was then calculated using an adaptation of the following calculation:

$$g_s = \frac{E \times p}{(e_i - e_a)} \qquad \text{(Equation 18)}$$

where g_s is stomatal conductance (mol m^{-2} s^{-1}), E is transpiration rate (mol m^{-2} s^{-1}), p is air pressure (kPa), e_a is atmospheric water vapor pressure (kPa) and e_i is water vapor pressure in the leaf intercellular space (kPa). We adapted the equation to:

$$g_i = \frac{J \times p}{(e_e - e_i)} \qquad \text{(Equation 19)}$$

where e_e is water vapor pressure at the equilibrium layer of the air-water interface in the leaf intercellular space (kPa), calculated as saturated vapor pressure at leaf temperature. Then, e_i

(kPa) was adjusted to the tested level of unsaturation within the leaf intercellular space (e_i = $e_e \times (RH_{cellular}/100)$). We then calculated intercellular resistance (mol m^{-2} s^{-1}) as:

$$r_i = \frac{1}{g_i} . \quad \text{(Equation 20)}$$

During the calculations, we assumed that the length of the diffusion pathway was equal to mean mesophyll thickness, and that the cross-sectional area of diffusion was equal to the cross-sectional area of a leaf exposed to evaporation, therefore r_i estimates were approximate. However, given that the r_i response to unsaturated e_i varies along a much smaller magnitude than the variability of r, the consequences of the described assumptions are unlikely consequential to this study, where r_i has been added to r when calculating ε_k (Equation **6**, **7**).

Statistical analyses

At Hyytiälä and in the large-scale dataset, linear mixed models (LMMs) with random intercepts were used to compare modelled to observed LWE. At Hyytiälä, the random intercept was sampling date, while in the larger dataset the random intercept was site ID with rank sampling time nested inside of site ID. Unadjusted Intraclass Correlations (ICC) were used to quantify unexplained variability between random factors which remained after modelled LWE was compared to observed LWE (Nakagawa, Johnson and Schielzeth, 2017). One outlier leaf water $\delta^{18}O$ measurement was removed from Hyytiälä data. Each LMM analysis was accompanied with a calculation of Root Mean Square Error (RMSE), which is an estimate of overall proximity of predicted LWE to observed LWE.

Results

Data Overview

Data used as input to the Craig-Gordon model to predict LWE at Hyytiälä were within the (Still *et al.,* 2022) range of the large-scale dataset (Fig. **1a-d**). Their means were lower at Hyytiälä compared to the large-scale dataset, most noticeably so for ^{2}H enrichment of water vapor above source water, which was 11.4‰ lower at Hyytiälä than in the large-scale dataset ($\Delta^{2}H_{wv}$, Fig. **1c**). Congruently, observed LWE at Hyytiälä was within the range of observed LWE in the large-scale dataset (Fig. **1e-f**). Nevertheless, mean observed $\Delta^{2}H_{lw}$ was approximately the same at Hyytiälä and in the large-scale dataset, while mean observed $\Delta^{18}O_{lw}$ was 2.4‰ higher at Hyytiälä than in the large-scale dataset (Fig. **1e-f**). The seasonal variability of leaf water isotope enrichment at Hyytiälä covered a substantial proportion of the data range in the large-scale dataset, at 34% for each of $\Delta^{2}H_{lw}$ and $\Delta^{18}O_{lw}$.

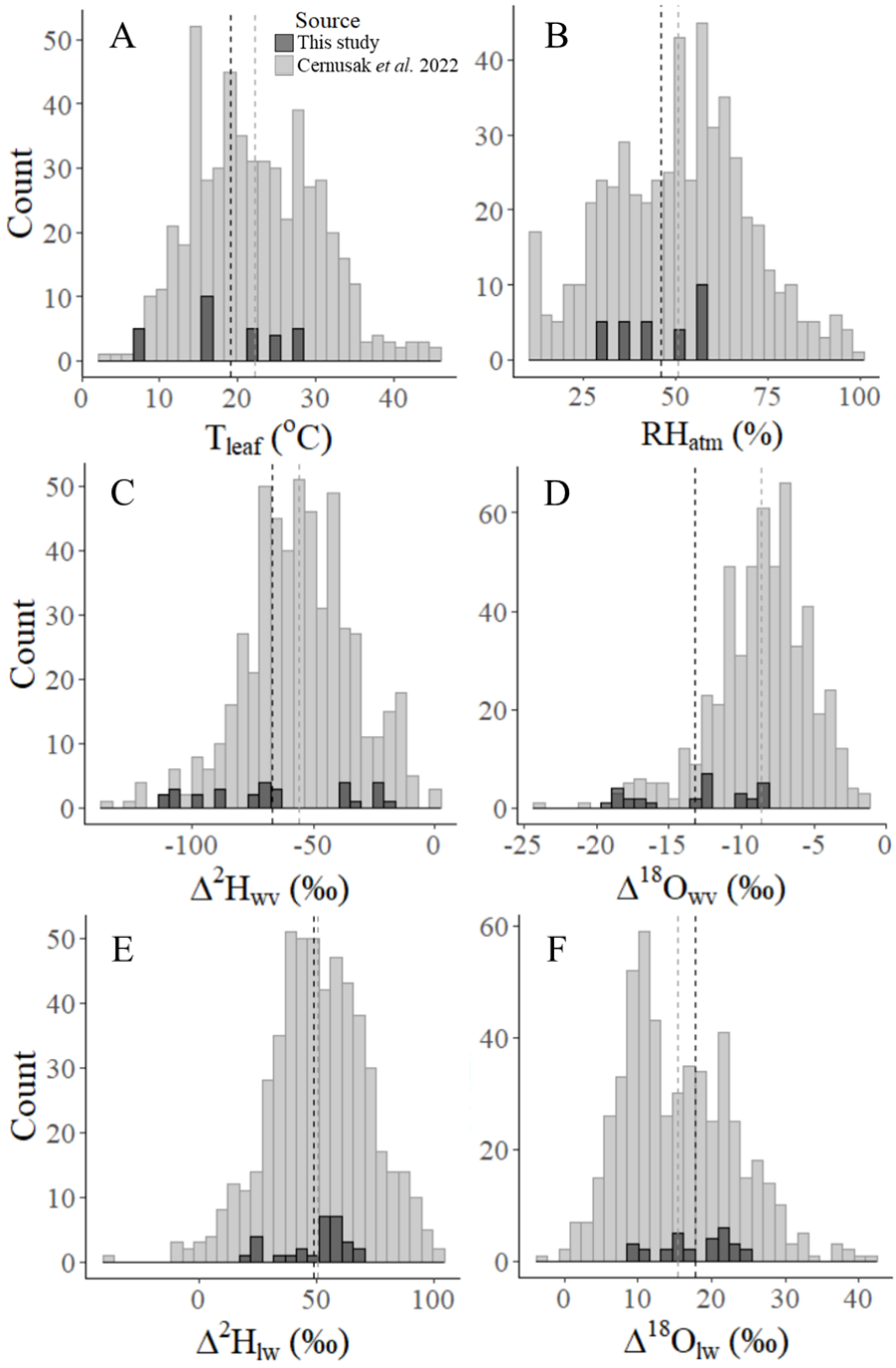

Figure 1. Frequency distributions of leaf temperature (T_{leaf} (ºC), A), atmospheric relative humidity (RH_{atm} (%), B), water vapor deuterium (Δ^2H_{wv} (‰), C) and oxygen-18 ($\Delta^{18}O_{wv}$ (‰), D) enrichment above source water, and observed leaf water deuterium (Δ^2H_{lw} (‰), E) and oxygen-18 ($\Delta^{18}O_{lw}$ (‰), F) enrichment above source water, n = 563. Data from this study (dark grey) shows seasonal variability for *P. sylvestris* during the 2019 growing season at Hyytiälä, Finland, and it overlays a selection of review data collected by Cernusak *et al.* (2022, lighter grey). Dashed lines show the mean of each parameter, for Hyytiälä and the review data.

Hypothesis 1: Increased influence of Δ_v and decreased influence of ε_k, by unsaturated e_i, is relevant to LWE

411 ***Hyytiälä***

412 *Foundational Craig-Gordon model*

413 When assumed $RH_{cellular}$ was lowered from 100% to 90% and 80%, predicted Δ^2H_{lw} and $\Delta^{18}O_{lw}$
414 became noticeably lower (red series in Fig. **2a-c**; Table **2**). This improved Δ^2H_{lw} predictions
415 by reducing the offset between observed and modelled values, because the predictions based
416 on 100% $RH_{cellular}$ largely overestimated Δ^2H_{lw} (red series in Fig. **2a**; Table **2**). However, for
417 $\Delta^{18}O_{lw}$, 100% $RH_{cellular}$ already provided a good agreement between the measured and modelled
418 $\Delta^{18}O_{lw}$, with only a modest average model overestimation of 1‰ (red series in Fig. **2e**). Hence,
419 the lowering of $RH_{cellular}$ to 90% or 80% led to increased error of $\Delta^{18}O_{lw}$ predictions, by
420 underestimation (red series in Fig. **2f-g**; Table **2**). The accuracy of LWE predictions was
421 affected by ±2ºC variability in T_{leaf} more for $\Delta^{18}O_{lw}$ than for Δ^2H_{lw}, and the impact was larger
422 on lower enrichments, for predictions by models with 100%, 90% and 80% $RH_{cellular}$ (horizontal
423 lines in Fig. **2a-c, e-g**).

424 When $RH_{cellular}$ was reduced to 90% or 80%, the lower predicted enrichments were lowered to
425 a larger extent than higher predicted enrichments, as indicated by the increase in intercepts and
426 the decline in slopes, for both elements (Fig. **2a-c, e-g**; Table **2**). This attribute meant that,
427 while reductions in $RH_{cellular}$ could reduce model prediction offsets from observed values if a
428 model otherwise overestimated LWE (Δ^2H_{lw}), they had a biased influence on model prediction
429 accuracy. Such a prediction accuracy bias was completely remediated for $\Delta^{18}O_{lw}$, by the model
430 optimization that found a fitted $RH_{cellular}$ that varied along a RH_{atm} gradient, albeit with an offset
431 between observed and measured values (Fig. **2 h**; Table **2**). Meanwhile, for Δ^2H_{lw} predictions,
432 the prediction accuracy bias was only partly remediated by fitted $RH_{cellular}$, because it improved
433 the prediction accuracy bias compared to 80% $RH_{cellular}$, but it worsened the prediction accuracy
434 bias compared to 90% $RH_{cellular}$ (Table **2**).

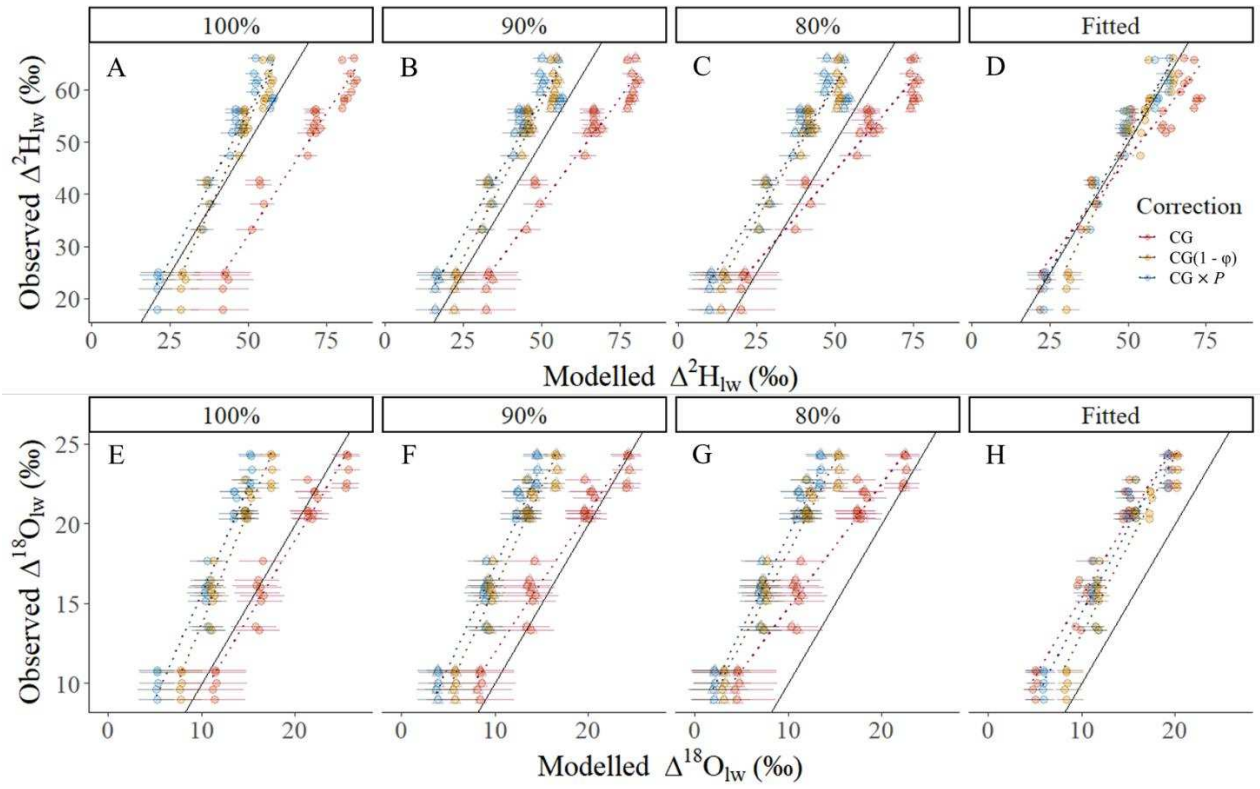

Figure 2. Relationships between modelled and measured Hyytiälä leaf water deuterium (Δ^2H_{lw}) and oxygen-18 ($\Delta^{18}O_{lw}$) enrichment, when leaf intercellular space relative humidity ($RH_{cellular}$) was changed in the models (100%, 90%, 80%, fitted $RH_{cellular}$. n = 29), to test unsaturated e_i effects to Δ^2H_{lw} and $\Delta^{18}O_{lw}$ via increased influence of Δ_v and decreased influence of ε_k to LWE. Dashed lines show linear mixed model fits, solid black lines demonstrate a 1:1 relationship, and horizontal lines show model variability in response to ±2ºC leaf temperature. Triangles in graphs with 90% and 80% $RH_{cellular}$ show model results once intercellular resistance (r_i) has been included in the calculation of ε_k. CG: Craig-Gordon model; CG(1 – φ): Craig-Gordon model with two-pool correction; CG × *P*: Craig-Gordon model with Péclet correction.

The fitted-$RH_{cellular}$ for $\Delta^{18}O_{lw}$ consistently underestimated observed $\Delta^{18}O_{lw}$, for the foundational CG model (Fig. **2 h**, Table **2**). Indeed, the Craig Gordon model assuming 100% $RH_{cellular}$ remained the best predictor of $\Delta^{18}O_{lw}$ (Fig. **2 e**, Table **2**). In contrast, for Δ^2H_{lw}, the fitted $RH_{cellular}$ exhibited reduced offsets between modelled and measured values, producing better Δ^2H_{lw} predictions compared to non-fitted $RH_{cellular}$, observed by a lowered Root Mean Square Error (RMSE) (Fig. **2 d**; Table **2**).

Performance of LWE models deteriorated extremely when only one of the two e_i occurrences in Equation **2** was adjusted for unsaturated e_i (Supplemental Table **1**), showing that the

448 relationships between e_i and both Δ_v and ε_k, are important to the response of LWE to
449 unsaturated e_i.

450 *Péclet and two-pool corrections*

451 Main results from this study can be derived from the foundational CG model, and results of
452 additional Péclet and two-pool corrections are described to demonstrate how such corrections
453 might interact with a decrease in e_i in Equation **2** tested for Hypothesis 1. Therefore, we used
454 one calculation of effective path length for the Péclet correction, and a literature-derived
455 constant φ for the two-pool correction.

456 The two-pool and Péclet correction almost always lowered Δ^2H_{lw} and $\Delta^{18}O_{lw}$ predictions
457 compared to the CG model and they had larger effects at higher enrichments, except for when
458 $RH_{cellular}$ was fitted (orange series in Fig. **2**; Table **2**). Resultantly, they mostly underestimated
459 Δ^2H_{lw} and $\Delta^{18}O_{lw,}$ but they still improved Δ^2H_{lw} predictions when $RH_{cellular}$ was 100%, 90%, or
460 fitted (RMSE in Table 2). The Péclet correction had less of an effect bias to higher enrichments
461 compared to the two-pool correction (blue series in Fig. **2**; Table **2**). Since the two-pool
462 correction, the Péclet correction and the lowered $RH_{cellular}$ all typically lowered predicted Δ^2H_{lw}
463 and $\Delta^{18}O_{lw}$, when the two-pool or Péclet correction were combined with lowered $RH_{cellular}$, they
464 led to even lower predicted Δ^2H_{lw} and $\Delta^{18}O_{lw}$ than if applied individually, except for when
465 $RH_{cellular}$ was fitted (Fig. **2**; Table **2**). Indeed, Δ^2H_{lw} was almost perfectly predicted, when
466 $RH_{cellular}$ was fitted after a Péclet correction had been applied (Fig. **2 d**; Table **2**). However,
467 unrealistically high fitted $RH_{cellular}$ were needed for the model optimization (103 – 146% and
468 105 – 210%, respectively; Supplemental Fig. **1**), showing that the versions of two-pool and
469 Péclet corrections used in this study were thus fundamentally incompatible with reductions in
470 $RH_{cellular}$ at Hyytiälä. Nevertheless, the larger effect to higher enrichments by the two-pool and
471 Péclet corrections balanced the larger effect to lower enrichments by $RH_{cellular}$ at 90% or 80%,

thus reducing resultant model prediction accuracy bias at different LWE, despite frequent underestimations.

Large-scale dataset

Results from the large-scale dataset were mostly parallel to results from Hyytiälä. Like at Hyytiälä, a reduction in $RH_{cellular}$ from 100%, to 90% and 80%, led to less enriched Δ^2H_{lw} and $\Delta^{18}O_{lw}$ predictions (Fig. **3**; Table **3**). Such reductions in predicted Δ^2H_{lw} and $\Delta^{18}O_{lw}$ clearly benefited Δ^2H_{lw} prediction accuracy by reducing overestimates, most evidently shown by a large decrease in RMSE of model predictions (Table **3**). These outcomes are the same as results observed for Hyytiälä (Table **2**). However, $\Delta^{18}O_{lw}$ prediction accuracy improved when $RH_{cellular}$ was lower than 100%, as shown by a decrease in RMSE (Table **3**), whereas $\Delta^{18}O_{lw}$ prediction accuracy decreased when $RH_{cellular}$ was lower than 100% at Hyytiälä (Table **2**). The larger decrease in predicted LWE at lower predicted enrichments when $RH_{cellular}$ was lowered from 100% to 90% or 80%, persisted beyond the Hyytiälä dataset to the large-scale dataset, for both elements (Fig. **3**; Table **3**). Like for Hyytiälä, this bias was mostly remediated for $\Delta^{18}O_{lw}$ by using a fitted $RH_{cellular}$ based on observed LWE and RH_{atm} (Fig. **3**; Table **3**). However, the fitted $RH_{cellular}$ also largely remediated the bias for Δ^2H_{lw}, unlike at Hyytiälä (Fig. **3**; Table **3**). In congruence with findings from Hyytiälä, the best-fitting model for Δ^2H_{lw} was the model with a fitted $RH_{cellular}$, while unlike at Hyytiälä, $\Delta^{18}O_{lw}$ was best explained by a model assuming 90% $RH_{cellular}$ rather than 100% $RH_{cellular}$. Overall, results from the large-scale dataset reinforce the observed relevance of reduced $RH_{cellular}$ to LWE observed at Hyytiälä, because they demonstrate that predictions of both Δ^2H_{lw} and $\Delta^{18}O_{lw}$ noticeably change, and even improve, in response to unsaturated e_i.

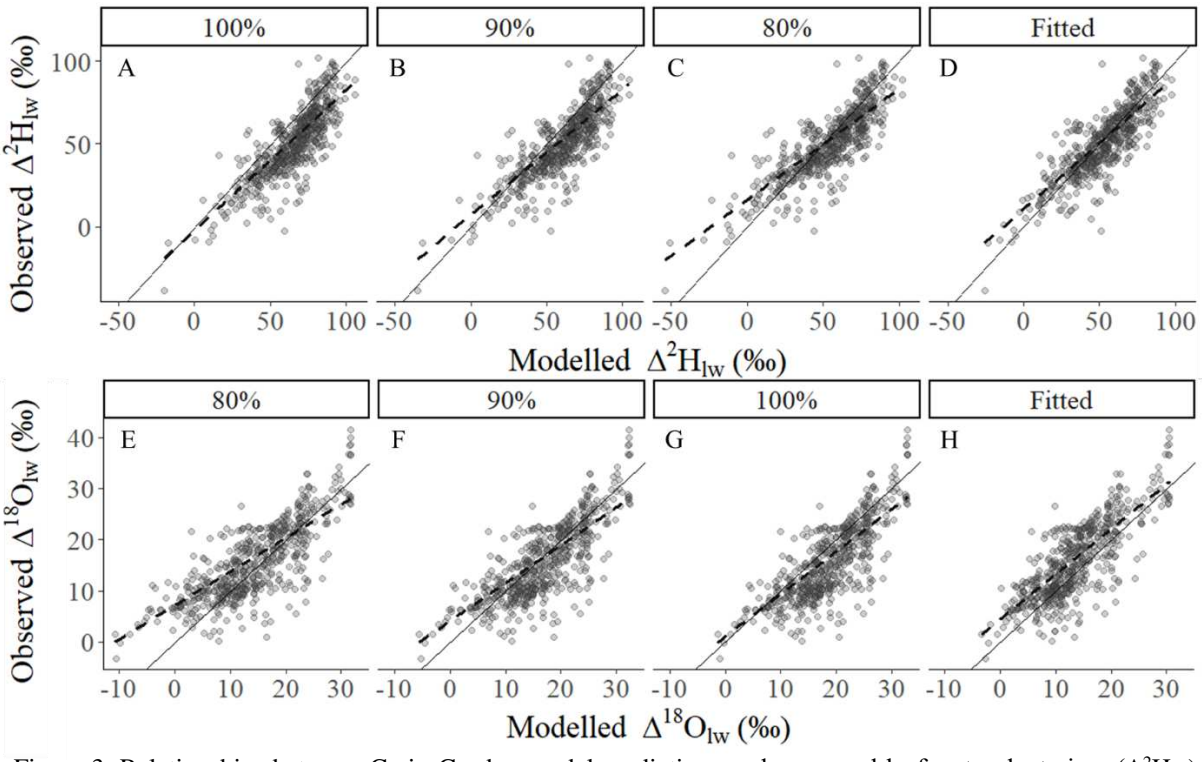

Figure 3. Relationships between Craig-Gordon model predictions and measured leaf water deuterium (Δ^2H_{lw}) and oxygen-18 ($\Delta^{18}O_{lw}$) enrichment with different assumptions of leaf intercellular space relative humidity (100%, 90%, 80%, fitted), in the studied large-scale dataset. The dataset includes data from this study combined with review data from Cernusak *et al.* (2022) (Mechanism 1, n = 563). Dashed lines show linear mixed model fits and solid lines demonstrate the 1:1 relationship.

Fitted $RH_{cellular}$ predictions

The fitted $RH_{cellular}$ increased as RH_{atm} increased (Fig. **4**). The fitted $RH_{cellular}$ for *P. sylvestris* at Hyytiälä was highly complementary to the fitted $RH_{cellular}$ for the larger dataset, as indicated by the almost overlapping fitted $RH_{cellular}$ along the common RH_{atm} gradient. Sensitivity tests for ±2ºC change in T_{leaf} showed that fitted $RH_{cellular}$ is influenced by ±2ºC changes in T_{leaf}, at both Hyytiälä and in the larger dataset (shaded regions in Fig. **4**).

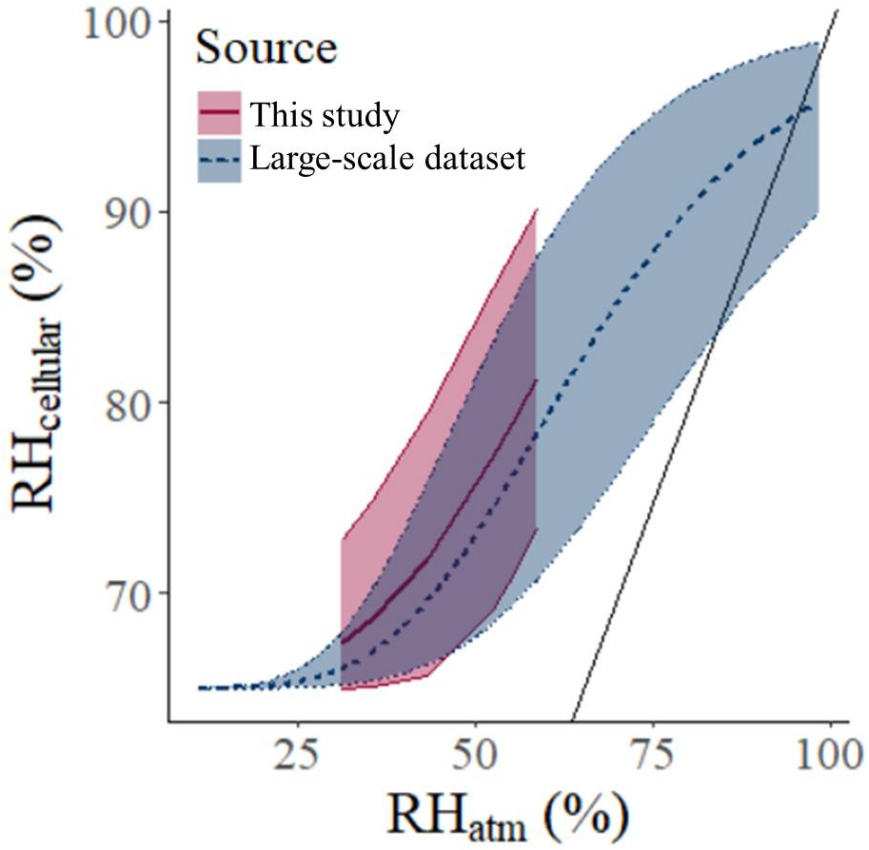

Figure 4. Fitted intercellular relative humidity ($RH_{cellular}$) in response to atmospheric RH (RH_{atm}) for *Pinus sylvestris* at Hyytiälä, Finland (n = 29, "This study"), and for the large-scale dataset which combines data from this study with review data from Cernusak *et al.* (2022) (n = 563, "Large-scale dataset"). The solid line demonstrates the 1:1 relationship, and shaded areas show fitted $RH_{cellular}$ sensitivity to ±2°C leaf temperature.

Hypothesis 2: Intercellular resistance fractionation irrelevant to LWE

At Hyytiälä, the isotope fractionation by decreased r and introduced intercellular resistance (r_i) from unsaturated e_i had a negligible influence on predicted Δ^2H_{lw} and $\Delta^{18}O_{lw}$, at $RH_{cellular}$ 90% and 80% (triangles strongly overlapped by circles in Figure 3 B, C, F & G). It changed ε_k estimates by less than 0.26 and 0.29 for Δ^2H_{lw} and $\Delta^{18}O_{lw}$, respectively, for 90% and 80% $RH_{cellular}$. Resultantly, it changed LWE by only 0 – 0.17‰ at 90% and 80% $RH_{cellular}$ for both Δ^2H_{lw} and $\Delta^{18}O_{lw}$.

Discussion

517 This study is the first to quantitatively evaluate the ecological relevance of unsaturated e_i to
518 LWE. Overall, results showed that unsaturated e_i effects is likely relevant to LWE by changing
519 LWE predictions, via both increased influence of Δ_v and decreased influence of ε_k (Fig. **2, 3**;
520 Table **2, 3,** Supplemental Table **1**). This means that it is necessary to consider unsaturated e_i as
521 an important source of error to LWE predictions and reconstructions from organic material,
522 albeit one which can be corrected. In this study, such corrections to e_i clearly benefited Δ^2H_{lw}
523 predictions, and conditionally benefited $\Delta^{18}O_{lw}$ predictions (Fig. **2, 3**; Table **2, 3**). Results
524 suggested that additional fractionation by concentration-driven diffusion in leaf intercellular
525 spaces (Equation **6**, **7**) is unlikely relevant to LWE.

526 **Correction for unsaturated e_i in studies that use leaf water isotopes**

527 Overall, when $RH_{cellular}$ and thus e_i was lowered in the foundational CG model, both Δ^2H_{lw} and
528 $\Delta^{18}O_{lw}$ predictions changed (Fig. **2**, **3**; Table **2**, **3**). Such changes improved Δ^2H_{lw} predictions
529 produced by the CG model because the offset between observed and measured Δ^2H_{lw}
530 decreased, at both Hyytiälä and in the large-scale dataset (RMSE in Table **2**, **3**). Meanwhile,
531 the benefits of lowered $RH_{cellular}$ were not clear for $\Delta^{18}O_{lw}$ because all reductions in $RH_{cellular}$ in
532 the CG model had effects too large for $\Delta^{18}O_{lw}$ predictions at Hyytiälä, while all reductions in
533 $RH_{cellular}$ in the CG model improved $\Delta^{18}O_{lw}$ predictions in the large-scale dataset compared to
534 the CG model assuming saturated e_i (RMSE in Table **2**, **3**). The more evident benefit to Δ^2H_{lw}
535 could have been because Δ^2H_{lw} can be strongly related to the isotopic disequilibrium between
536 water vapor and source water, which was changed by the reductions in $RH_{cellular}$ tested in this
537 study, while $\Delta^{18}O_{lw}$ is more strongly related to RH_{atm} (Munksgaard *et al.*, 2017; Cernusak *et*
538 *al.*, 2022). These results show how it is potentially valuable to account for unsaturated e_i during
539 Δ^2H_{lw} predictions and Δ^2H_{lw} reconstructions from plant compounds, such as tree rings or *n*-
540 alkanes, because unsaturated e_i directly affects the factors known to be most strongly related
541 to Δ^2H_{lw}.

When using a constant lowered $RH_{cellular}$ (90% or 80%), model bias increased, because the reduced $RH_{cellular}$ affected lower predicted LWE more than higher predicted LWE for both Δ^2H_{lw} and $\Delta^{18}O_{lw}$ (Fig. **2**, **3**; Table **2**, **3**). It is noteworthy to recognize that this means that when 100% $RH_{cellular}$ is being used when intercellular spaces are unsaturated, then it thus brings a model prediction accuracy bias of its own. This shows that it is valuable to start using a variable $RH_{cellular}$ along a range of LWE values when calculating e_i, which is supported by evidence that $RH_{cellular}$ changes (Cernusak *et al.*, 2018; Wong *et al.*, 2022). When results from this study are combined with measurements of $RH_{cellular}$ responses to VPD from Cernusak et al. (2018), a viable solution for estimating $RH_{cellular}$ is calculating $RH_{cellular}$ from RH_{atm} or atmospheric VPD, which are negatively correlated to one another. More studies like Cernusak et al. (2018) are required to gather species-specific $RH_{cellular}$ responses to changing RH_{atm} or VPD, their study can be used to tentatively estimate e_i of two species: *Juniperus monosperma* and *Pinus edulis*, in response to changing VPD. Otherwise, we suggest using the following equation to estimate e_i:

$$e_i = 0.65 + \frac{0.35}{(1+A \times e^{-B \times RH_{atm}})^{\frac{1}{C}}}$$

wherein generalized suggested parameters are: A = 2.03, B = 5.179, and C = 0.096, based on fitted $RH_{cellular}$ from the large-scale dataset. More details can be found in the methods section (Equation **14**). The large-scale dataset is a collection of different plant functional groups, and such diversity in the dataset could affect fitted $RH_{cellular}$, perhaps more so at the upper and lower $RH_{cellular}$ limits. For example, variability in stomatal conductance could be responsible for extremely low fitted $RH_{cellular}$ at low RH_{atm}, therefore it is likely important to incorporate non-steady state modelling in future studies when RH_{atm} is low. The correction can be refined to specific ecological contexts using site-specific and species-specific information, for example, by calculating a fitted $RH_{cellular}$ based on an existing study of the same species in a similar

location, like this study evaluated Scots pine at Hyytiälä. Or, ideally, A and B are refined based on experimental data on species-specific $RH_{cellular}$ responses to RH_{atm} or VPD. Indeed, these are suggested starting points for correcting e_i for its unsaturation when predicting or reconstructing LWE.

The model optimization estimated that fitted $RH_{cellular}$ for optimal LWE predictions would reach much lower $RH_{cellular}$ than what has been empirically measured by Cernusak *et al.* (2018) and Wong *et al.* (2022), especially at low RH_{atm} (Fig. **4**). When the optimization was adjusted to limit fitted $RH_{cellular}$ to measured values, the fitted $RH_{cellular}$ for Hyytiälä was bounded to 80% across all measured RH_{atm} at Hyytiälä, which predicted $\Delta^{18}O_{lw}$ poorly (Fig. **2G**; Table **2**). At low RH_{atm}, the extremely low fitted $RH_{cellular}$ could have been affected by increased stomatal closure, because stomatal closure disrupts the hypothesized relationship between RH_{atm} and $RH_{cellular}$. Also, if $\Delta^{18}O_{lw}$ was fitted separately to $\Delta^{2}H_{lw}$ then the fitted $RH_{cellular}$ of $\Delta^{18}O_{lw}$ is closer to empirical measurements of $RH_{cellular}$ by Cernusak et al. (2018) and Wong *et al.* (2022), especially at Hyytiälä (Supplemental Fig. **2**). A potential reason for such low fitted $RH_{cellular}$ for $\Delta^{2}H_{lw}$, is that the CG model did not predict $\Delta^{2}H_{lw}$ as accurately as $\Delta^{18}O_{lw}$ in this study (Fig. **2**, **3**; Table **2**, **3**). Therefore, a lower fitted $RH_{cellular}$ for $\Delta^{2}H_{lw}$ might have been necessary to remediate other sources of error in the CG model for $\Delta^{2}H_{lw}$. An alternative fitted $RH_{cellular}$ to correct for unsaturated e_i for $\Delta^{18}O_{lw}$ only, is based on separate fitting of $RH_{cellular}$ for $\Delta^{18}O_{lw}$ in the large-scale dataset (A =1088.18, B = 9.81 and C = 3.06, Suppplemental Fig. **2**).

Results suggested that T_{leaf} is important to consider alongside accounting for unsaturated e_i in future studies, because fitted $RH_{cellular}$ is sensitive to ±2ºC variability in T_{leaf} (Fig. **4**). Cryogenic water extraction artefacts, and xylem sampling effects, may also affect LWE values (Chen *et al.*, 2020; Barbeta *et al.*, 2022; Diao *et al.*, 2022; Nehemy *et al.*, 2022).

When applying the Péclet correction, L is dependent on assumptions in the CG model (Table **1**; Loucos et al. (2014)). In this study, we tested assumptions that could affect the calculation of L. Also, the Péclet and two-pool corrections can affect the accuracy of Δ^2H_{lw} and $\Delta^{18}O_{lw}$ predictions differently (Bögelein, Thomas and Kahmen, 2017). Therefore, it is understandable that in this study, the selected Péclet and two-pool corrections were favorable to only a minority of scenarios (Fig. **2**; Table **2**). Importantly, we have shown that it is necessary to develop co-implementation of the two-pool and Péclet with unsaturated e_i further, because the versions used in this study were incompatible with unsaturated e_i effects to $\frac{e_a}{e_i}$ of the CG model (Equation **2;** Fig. **2**; Table **2**). After all, when $RH_{cellular}$ was fitted after the two-pool and Péclet corrections, the fitted $RH_{cellular}$ became unrealistically high (103 – 146% and 105 – 210%, respectively, Supplemental Fig. **1**). It is worthwhile to further explore the co-implementation of two-pool and Péclet corrections alongside adjustments for unsaturated e_i, because Péclet and two-pool corrections have potential to remediate model prediction accuracy bias introduced by unsaturated e_i via $\frac{e_a}{e_i}$ of the CG model (Fig. **2**; Table **2**).

Unsaturated e_i effects to fractionation within ε_k

Results from this study showed that it is not necessary to further explore the effect of unsaturated e_i to fractionation within ε_k, by decreased r and introduced r_i, for 80 – 100% $RH_{cellular}$, because it had a negligible effect to predicted Δ^2H_{lw} and $\Delta^{18}O_{lw}$ (< 0.17‰, Fig. **2 B**, **C**, **F**, **G**). A contributing factor to this finding, is that the influence of ε_k to LWE decreases in response to unsaturated e_i, as observed for Hypothesis 1. Therefore, intercellular resistance (r_i) does not need to be incorporated into the calculation of ε_k in response to unsaturated e_i, unless the calculation of ε_k receives major revision in the future. There is opportunity for future investigations to explore how different calculation techniques for g_s might be affected by unsaturated e_i (see Damour *et al.*, 2010).

Conclusion

Our results show that accounting for unsaturated e_i changes spatiotemporal LWE predictions and can even improve them. We therefore conclude that unsaturated e_i should be considered as a key modification factor of leaf water stable isotopes in future studies. Particularly, to account for higher influence of Δ_v and lower influence of ε_k by decreasing e_i in $\frac{e_a}{e_i}$ of the CG model (Equation **2**). Corrections which use a constant value of $RH_{cellular}$ when calculating $\frac{e_a}{e_i}$ are not effective, likewise it is ineffective to continue to use a constant $RH_{cellular}$ of 100%, when e_i is assumed to be saturated. We propose a model correction for both Δ^2H_{lw} and $\Delta^{18}O_{lw}$ based on RH_{atm}, and we suggest that such an approach can alternatively be applied with VPD. This model correction is a starting point for more accurately predicting LWE or reconstructing LWE from plant-derived organic proxies such as tree rings and *n*-alkanes. This may particularly benefit ^2H interpretations, due to the noticeable improvement on Δ^2H_{lw} predictions by lowered $RH_{cellular}$ during LWE modelling, but it may not benefit ^{18}O interpretations.

Acknowledgements

Many thanks to Elina Sahlstedt, Giles Young, Kersti Leppä, Eloise Angove, Magdalena Drys, Aleksi Lehtonen, Yann Salmon, Daniel Zannoni and three anonymous reviewers for constructive comments, to Juha Heikkinen for statistical consultation, to Pasi Kolari for providing leaf cuvette gas exchange data, to Aino Seppänen for water extractions and to Daniel Nelson for performing stable isotope measurements.

Funding

633 This work was supported by the Academy of Finland (#295319, #341984, #343059), the
634 Academy of Finland Flagship Program (#337549), the Kone Foundation (#202006108), the
635 Swiss National Science Foundation (#179978) and the European Research Council (#755865).

636 Author contributions

637 YT, PS-A, KTR-G, PK & JB planned, facilitated and/or conducted field work at Hyytiälä. The
638 subsequent manuscript idea was realized by CA, KTR-G, ML & MS. Data processing, isotope
639 modelling, and analyses were conducted by CA and O-PT. CA was responsible for writing the
640 manuscript, with major contributions from KTR-G, ML, MS, YT, AK, O-PT and all authors
641 contributed to the writing of the manuscript.

642 Data availability

643 Review data used in this study is freely available online thanks to Cernusak *et al.* (2022). The
644 data from Hyytiälä which support findings from this study will be made freely available.

645 Competing interests

646 None declared.

647 Supplemental Materials

648 **Supplemental Table 1** Linear mixed model fits between modelled and observed leaf water
649 deuterium (Δ^2H_{lw}) and oxygen-18 ($\Delta^{18}O_{lw}$) when intercellular relative humidity ($RH_{cellular}$) has
650 been adjusted in association with, either, enrichment of atmospheric vapor relative to source
651 water (Δ^2H_{wv} or $\Delta^{18}O_{wv}$), or, the kinetic fractionation during diffusion through the stomata and
652 boundary layer (ε_k) in the Craig Gordon model.

Supplemental Fig. 1 Fitted leaf intercellular space relative humidity, in response to atmospheric relative humidity, with different corrections for leaf water heavy isotope enrichment modelling.

Supplemental Fig. 2 Fitted leaf intercellular relative humidity, in response to atmospheric relative humidity, separately fitted for each of $\Delta^{18}O_{lw}$ and $\Delta^{2}H_{lw}$.

References

Aalto, J. *et al.* (2014) 'New foliage growth is a significant, unaccounted source for volatiles in boreal evergreen forests', *Biogeosciences*, 11(5). Available at: https://doi.org/10.5194/bg-11-1331-2014.

Allison, G.B., Gat, J.R. and Leaney, F.W.J. (1985) 'The relationship between deuterium and oxygen-18 delta values in leaf water', *Chemical Geology: Isotope Geoscience Section*, 58(1–2). Available at: https://doi.org/10.1016/0168-9622(85)90035-1.

Barbeta, A. *et al.* (2022) 'Evidence for distinct isotopic compositions of sap and tissue water in tree stems: consequences for plant water source identification', *New Phytologist*, 233(3). Available at: https://doi.org/10.1111/nph.17857.

Bariac, T. *et al.* (1989) 'Evaluating water fluxes of field-grown alfalfa from diurnal observations of natural isotope concentrations, energy budget and ecophysiological parameters', *Agricultural and Forest Meteorology*, 48(3–4). Available at: https://doi.org/10.1016/0168-1923(89)90073-7.

Bögelein, R., Thomas, F.M. and Kahmen, A. (2017) 'Leaf water 18O and 2H enrichment along vertical canopy profiles in a broadleaved and a conifer forest tree', *Plant Cell and Environment*, 40(7). Available at: https://doi.org/10.1111/pce.12895.

Buckley, T.N. and Sack, L. (2019) 'The humidity inside leaves and why you should care: implications of unsaturation of leaf intercellular airspaces', *American Journal of Botany*, 106(5). Available at: https://doi.org/10.1002/ajb2.1282.

Canny, M.J. and Huang, C.X. (2006) 'Leaf water content and palisade cell size', *New Phytologist*, 170(1). Available at: https://doi.org/10.1111/j.1469-8137.2005.01633.x.

Cernusak, L.A. *et al.* (2016) 'Stable isotopes in leaf water of terrestrial plants', *Plant Cell and Environment*. Available at: https://doi.org/10.1111/pce.12703.

Cernusak, L.A. *et al.* (2018) 'Unsaturation of vapour pressure inside leaves of two conifer species', *Scientific Reports*, 8(1). Available at: https://doi.org/10.1038/s41598-018-25838-2.

Cernusak, L.A. *et al.* (2022) 'Do 2H and 18O in leaf water reflect environmental drivers differently?', *New Phytologist*, 235(1). Available at: https://doi.org/10.1111/nph.18113.

Cernusak, L.A. and Kahmen, A. (2013) 'The multifaceted relationship between leaf water 18O enrichment and transpiration rate', *Plant, Cell and Environment*, 36(7). Available at: https://doi.org/10.1111/pce.12081.

Chen, Y. *et al.* (2020) 'Stem water cryogenic extraction biases estimation in deuterium isotope composition of plant source water', *Proceedings of the National Academy of Sciences of the United States of America*, 117(52). Available at: https://doi.org/10.1073/PNAS.2014422117.

Craig, H. and G.L.I. (1965) 'Isotope oceanography: Deuterium and oxygen 18 variations in the ocean and the marine atmosphere', in *Symposium on Marine Geochemistry*.

Cueni, F. *et al.* (2021) 'Using plant physiological stable oxygen isotope models to counter food fraud', *Scientific Reports*, 11(1). Available at: https://doi.org/10.1038/s41598-021-96722-9.

Damour, G., Simonneau, T., Cochard, H., & Urban, L. (2010). An overview of models of stomatal conductance at the leaf level. In Plant, Cell and Environment (Vol. 33, Issue 9). https://doi.org/10.1111/j.1365-3040.2010.02181.x

Diao, H. *et al.* (2022) 'Technical note: On uncertainties in plant water isotopic composition following extraction by cryogenic vacuum distillation', *Hydrology and Earth System Sciences*, 26(22). Available at: https://doi.org/10.5194/hess-26-5835-2022.

Dongmann, G. *et al.* (1974) 'On the enrichment of H218O in the leaves of transpiring plants', *Radiation and Environmental Biophysics*, 11(1). Available at: https://doi.org/10.1007/BF01323099.

Farquhar, G. D., Firth, P. M., Wetselaar, R., & Weir, B. (1980). On the Gaseous Exchange of Ammonia between Leaves and the Environment: Determination of the Ammonia Compensation Point. Plant Physiology, 66(4). https://doi.org/10.1104/pp.66.4.710

Farquhar, G.D. *et al.* (1989) 'Carbon Isotope Fractionation and Plant Water-Use Efficiency', in. Available at: https://doi.org/10.1007/978-1-4612-3498-2_2.

Farquhar, G.D., Cernusak, L.A. and Barnes, B. (2007) 'Heavy water fractionation during transpiration', *Plant Physiology*. Available at: https://doi.org/10.1104/pp.106.093278.

Farquhar, G.D. and Lloyd, J. (1993) 'Carbon and Oxygen Isotope Effects in the Exchange of Carbon Dioxide between Terrestrial Plants and the Atmosphere', in *Stable Isotopes and Plant Carbon-water Relations*. Available at: https://doi.org/10.1016/b978-0-08-091801-3.50011-8.

Farquhar, G.D. and Raschke, K. (1978) 'On the Resistance to Transpiration of the Sites of Evaporation within the Leaf', *Plant Physiology*, 61(6). Available at: https://doi.org/10.1104/pp.61.6.1000.

720 Flanagan, L.B. and Ehleringer, J.R. (1991) 'Stable Isotope Composition of Stem and Leaf
721 Water: Applications to the Study of Plant Water Use', *Functional Ecology*, 5(2). Available at:
722 https://doi.org/10.2307/2389264.

723 Gessler, A. *et al.* (2009) 'Tracing carbon and oxygen isotope signals from newly assimilated
724 sugars in the leaves to the tree-ring archive', *Plant, Cell and Environment*, 32(7). Available
725 at: https://doi.org/10.1111/j.1365-3040.2009.01957.x.

726 Gessler, A. *et al.* (2018) 'Drought induced tree mortality – a tree-ring isotope based
727 conceptual model to assess mechanisms and predispositions', *New Phytologist*. Available at:
728 https://doi.org/10.1111/nph.15154.

729 Hartl-Meier, C. *et al.* (2014) 'Uniform climate sensitivity in tree-ring stable isotopes across
730 species and sites in a mid-latitude temperate forest', *Tree Physiology*, 35(1). Available at:
731 https://doi.org/10.1093/treephys/tpu096.

732 Hepp, J. *et al.* (2017) 'Late Quaternary relative humidity changes from Mt. Kilimanjaro,
733 based on a coupled 2H-18O biomarker paleohygrometer approach', *Quaternary*
734 *International*, 438. Available at: https://doi.org/10.1016/j.quaint.2017.03.059.

735 Holloway-Phillips, M. *et al.* (2022) 'Species variation in the hydrogen isotope composition of
736 leaf cellulose is mostly driven by isotopic variation in leaf sucrose', *Plant Cell and*
737 *Environment*, 45(9). Available at: https://doi.org/10.1111/pce.14362.

738 Horita, J., Rozanski, K. and Cohen, S. (2008) 'Isotope effects in the evaporation of water: A
739 status report of the Craig-Gordon model', in *Isotopes in Environmental and Health Studies*.
740 Available at: https://doi.org/10.1080/10256010801887174.

741 Jarvis, P.G. and Slatyer, R.O. (1970) 'The role of the mesophyll cell wall in leaf
742 transpiration', *Planta*, 90(4). Available at: https://doi.org/10.1007/BF00386383.

743 Kahmen, A. *et al.* (2011) 'Cellulose δ18O is an index of leaf-to-air vapor pressure difference
744 (VPD) in tropical plants', *Proceedings of the National Academy of Sciences of the United*
745 *States of America*, 108(5). Available at: https://doi.org/10.1073/pnas.1018906108.

746 Kim, Y. *et al.* (2018) 'Thermal infrared imaging of conifer leaf temperatures: Comparison to
747 thermocouple measurements and assessment of environmental influences', *Agricultural and*
748 *Forest Meteorology*, 248. Available at: https://doi.org/10.1016/j.agrformet.2017.10.010.

749 Kolari, P. *et al.* (2012) 'Evaluation of accuracy in measurements of VOC emissions with
750 dynamic chamber system', *Atmospheric Environment*, 62. Available at:
751 https://doi.org/10.1016/j.atmosenv.2012.08.054.

752 Kolari, P. *et al.* (2022) *Hyytiälä SMEAR II site characteristics*, *[Data set]*. Available at:
753 https://dspace.uef.fi/handle/123456789/26786 (Accessed: 16 February 2023).

754 Launiainen, S. *et al.* (2016) 'Do the energy fluxes and surface conductance of boreal
755 coniferous forests in Europe scale with leaf area?', *Global Change Biology*, 22(12). Available
756 at: https://doi.org/10.1111/gcb.13497.

757 Leaney, F.W. *et al.* (1985) 'Hydrogen-isotope composition of leaf water in C3 and C4 plants:
758 its relationship to the hydrogen-isotope composition of dry matter', *Planta*, 164(2). Available
759 at: https://doi.org/10.1007/BF00396084.

760 Lehmann, M.M. *et al.* (2018) 'The effect of 18O-labelled water vapour on the oxygen isotope
761 ratio of water and assimilates in plants at high humidity', *New Phytologist*, 217(1). Available
762 at: https://doi.org/10.1111/nph.14788.

763 Lehmann, M.M. *et al.* (2021) 'More than climate: Hydrogen isotope ratios in tree rings as
764 novel plant physiological indicator for stress conditions', *Dendrochronologia*, 65. Available
765 at: https://doi.org/10.1016/j.dendro.2020.125788.

766 Leppä, K. *et al.* (2022) 'Explicitly accounting for needle sugar pool size crucial for predicting
767 intra-seasonal dynamics of needle carbohydrates δ18O and δ13C.', *New Phytologist*, 236(6),
768 pp. 2044–2060.

769 Loucos, K.E. *et al.* (2014) 'Observed relationships between leaf H218O Péclet effective
770 length and leaf hydraulic conductance reflect assumptions in Craig-Gordon model
771 calculations', *Tree Physiology*, 35(1). Available at: https://doi.org/10.1093/treephys/tpu110.

772 Merlivat, L. (1978). Molecular diffusivities of H216O, HD16O, and H218O in gases. The
773 Journal of Chemical Physics, 69(6). https://doi.org/10.1063/1.436884

774 Munksgaard, N.C. *et al.* (2017) 'Identifying drivers of leaf water and cellulose stable isotope
775 enrichment in Eucalyptus in northern Australia', *Oecologia*, 183(1). Available at:
776 https://doi.org/10.1007/s00442-016-3761-8.

777 Nakagawa, S., Johnson, P.C.D. and Schielzeth, H. (2017) 'The coefficient of determination
778 R2 and intra-class correlation coefficient from generalized linear mixed-effects models
779 revisited and expanded', *Journal of the Royal Society Interface*, 14(134). Available at:
780 https://doi.org/10.1098/rsif.2017.0213.

781 Nehemy, M.F. *et al.* (2022) 'Phloem water isotopically different to xylem water: Potential
782 causes and implications for ecohydrological tracing', *Ecohydrology*, 15(3). Available at:
783 https://doi.org/10.1002/eco.2417.

784 Newberry, S.L., Nelson, D.B. and Kahmen, A. (2017) 'Cryogenic vacuum artifacts do not
785 affect plant water-uptake studies using stable isotope analysis', *Ecohydrology*, 10(8).
786 Available at: https://doi.org/10.1002/eco.1892.

787 Nobel, P.S. (2005) *Physicochemical and Environmental Plant Physiology, Third Edition*,
788 *Physicochemical and Environmental Plant Physiology, Third Edition*. Available at:
789 https://doi.org/10.1016/B978-0-12-520026-4.X5000-8.

790 Pirinen, P. *et al.* (2012) *Climatological statistics of Finland 1981-2010*, *Reports*.

791 R Core Team (2022) 'R: A language and environment for statistical computing'. Vienna,
792 Austria: R Foundation for Statistical Computing. Available at: https://www.R-project.org/
793 (Accessed: 19 January 2023).

794 Roden, J. *et al.* (2015) 'The enigma of effective path length for 18O enrichment in leaf water
795 of conifers', *Plant Cell and Environment*, 38(12). Available at:
796 https://doi.org/10.1111/pce.12568.

797 Sachse, D. *et al.* (2012) 'Molecular paleohydrology: Interpreting the hydrogen-isotopic
798 composition of lipid biomarkers from photosynthesizing organisms', *Annual Review of Earth
799 and Planetary Sciences*, 40. Available at: https://doi.org/10.1146/annurev-earth-042711-
800 105535.

801 Sharkey, T.D. *et al.* (1982) ' A Direct Confirmation of the Standard Method of Estimating
802 Intercellular Partial Pressure of CO 2 ', *Plant Physiology*, 69(3). Available at:
803 https://doi.org/10.1104/pp.69.3.657.

804 Snyder, K.A. *et al.* (2010) 'Diurnal variations of needle water isotopic ratios in two pine
805 species', *Trees - Structure and Function*, 24(3). Available at: https://doi.org/10.1007/s00468-
806 010-0429-6.

807 Song, X. *et al.* (2015) 'Measurements of transpiration isotopologues and leaf water to assess
808 enrichment models in cotton', *New Phytologist*, 206(2). Available at:
809 https://doi.org/10.1111/nph.13296.

810 Soudant, A. *et al.* (2016) 'Intra-annual variability of wood formation and δ13C in tree-rings
811 at Hyytiälä, Finland', *Agricultural and Forest Meteorology*, 224. Available at:
812 https://doi.org/10.1016/j.agrformet.2016.04.015.

813 Still, C.J. *et al.* (2022) 'No evidence of canopy-scale leaf thermoregulation to cool leaves
814 below air temperature across a range of forest ecosystems', *Proceedings of the National
815 Academy of Sciences of the United States of America*, 119(38). Available at:
816 https://doi.org/10.1073/pnas.2205682119.

817 Tang, Y. *et al.* (2022) 'Tree organ growth and carbon allocation dynamics impact the
818 magnitude and δ13C signal of stem and soil CO2fluxes', *Tree Physiology*, 42(12). Available
819 at: https://doi.org/10.1093/treephys/tpac079.

820 Treydte, K. *et al.* (2014) 'Seasonal transfer of oxygen isotopes from precipitation and soil to
821 the tree ring: Source water versus needle water enrichment', *New Phytologist*, 202(3).
822 Available at: https://doi.org/10.1111/nph.12741.

823 Vesala, T. *et al.* (2017) 'Effect of leaf water potential on internal humidity and CO2
824 dissolution: Reverse transpiration and improved water use efficiency under negative
825 pressure', *Frontiers in Plant Science*, 8(FEBRUARY). Available at:
826 https://doi.org/10.3389/fpls.2017.00054.

827 Vitali, V. *et al.* (2022) 'The unknown third – Hydrogen isotopes in tree-ring cellulose across
828 Europe', *Science of the Total Environment*, 813. Available at:
829 https://doi.org/10.1016/j.scitotenv.2021.152281.

830 Voelker, S.L. *et al.* (2014) 'Reconstructing relative humidity from plant δ18O and δD as
831 deuterium deviations from the global meteoric water line', *Ecological Applications*, 24(5).
832 Available at: https://doi.org/10.1890/13-0988.1.

833 Walker, C.D. *et al.* (1989) 'The influence of transpiration on the equilibration of leaf water
834 with atmospheric water vapour', *Plant, Cell & Environment*, 12(3). Available at:
835 https://doi.org/10.1111/j.1365-3040.1989.tb01937.x.

836 West, A.G., Patrickson, S.J. and Ehleringer, J.R. (2006) 'Water extraction times for plant and
837 soil materials used in stable isotope analysis', *Rapid Communications in Mass Spectrometry*,
838 20(8). Available at: https://doi.org/10.1002/rcm.2456.

839 Wong, S.C. *et al.* (2022) 'Humidity gradients in the air spaces of leaves', *Nature Plants*, 8(8).
840 Available at: https://doi.org/10.1038/s41477-022-01202-1.

841 Zannoni, D. *et al.* (2022) 'Non-Equilibrium Fractionation Factors for D/H and 18O/16O
842 During Oceanic Evaporation in the North-West Atlantic Region', *Journal of Geophysical*
843 *Research: Atmospheres*, 127(21). Available at: https://doi.org/10.1029/2022JD037076.

844

845

846

847

848

849

850

851

Tables

Table 1. Abbreviations and symbols.

Abbreviation	Description
LWE	Leaf water heavy isotope enrichment
δ^2H	Isotope ratio of ^2H compared to ^1H, relative to VSMOW (‰, Equation **4**)
$\delta^{18}O$	Isotope ratio of ^{18}O compared to ^{16}O, relative to VSMOW (‰, Equation **4**)
RH_{atm}	Atmospheric relative humidity (%)
$RH_{cellular}$	Relative humidity within leaf intercellular spaces (%)
$\Delta^{18}O_{lw}$	Leaf water ^{18}O enrichment above source (xylem/twig) water (‰, Equation **5**)
Δ^2H_{lw}	Leaf water ^2H enrichment above source (xylem/twig) water (‰, Equation **5**)
e_i	Leaf intercellular water vapor pressure (kPa)
ε_k	Combined kinetic fractionation factor for diffusion of water vapor through the stomata and leaf boundary layer. This study explores additional fractionation by n_i within ε_k.
Δ_v	Isotopic enrichment of atmospheric water vapor from source water (Equation **5**)
L	Effective path length for the Péclet effect
T_{leaf}	Leaf temperature (°C)
T_{atm}	Atmospheric temperature (°C)
g_s	Stomatal conductance ($molm^{-2}s^{-1}$)
GFWL	Gross foliar water loss; all foliar water loss
GFWU	Gross foliar water uptake; all foliar water uptake
Ψ	Water potential (mPa)
r	Stomatal resistance ($molm^{-2}s^{-1}$)
r_b	Boundary layer resistance ($molm^{-2}s^{-1}$)
r_i	Intercellular resistance ($molm^{-2}s^{-1}$) (Supplemental Methods **2**)
φ	Proportion of unenriched xylem water in leaf water for the two-pool correction
VPD	Vapor pressure deficit (kPa)
RMSE	Root Mean Square Error. An estimate for overall proximity of predictions to observations.
CG	Craig Gordon leaf water heavy isotope enrichment model (Equation **2**)
CG(1 - φ)	Craig-Gordon derived leaf water heavy isotope enrichment model with two-pool correction applied (Methods **S1**)
CG × P	Craig-Gordon derived leaf water heavy isotope enrichment model with Péclet correction applied (Methods **S1**)
R^2(M)	Marginal R^2. A pseudo-R^2 estimate for the models being tested
R^2(C)	Conditional R^2. A pseudo-R^2 estimate for the models being tested combined with model random effects, such as sampling date, time, and site
ICC	Intraclass Correlation. The probability that two values from the same sampling date and time, and/or site, correlate, on a scale of 0-1.

Table 2. Linear mixed model fits between modelled and observed leaf water deuterium (Δ^2H_{lw}) and oxygen-18 ($\Delta^{18}O_{lw}$) enrichment at Hyytiälä (n = 29), with models using different intercellular relative humidity ($RH_{cellular}$, %, Mechanism 1. CG: Craig-Gordon model; CG(1 - φ): Craig-Gordon model with two-pool correction; CG × *P*: Craig-Gordon model with Péclet correction; R^2(M): Marginal R^2; R^2(C): Conditional R^2; ICC: Intraclass correlation between sampling dates).

	Model correction	$RH_{cellular}$ (%)	Intercept	Slope[a]	ICC	R^2(M)	R^2(C)	RMSE
Hyytiälä Δ^2H_{lw}	CG	100	-14.26 ± 3.88	**0.93** ± 0.06	0.01	0.95	0.96	19.27
	CG(1 - φ)		-14.26 ± 3.88	**1.36** ± 0.08	0.01	0.95	0.96	5.44
	CG × *P*		-1.29 ± 4.55	**1.14** ± 0.1	0.03	0.93	0.96	6.37
	CG	90	-2.26 ± 2.67	**0.81** ± 0.04	0.01	0.95	0.96	14.52
	CG(1 - φ)		-2.26 ± 2.67	**1.19** ± 0.06	0.01	0.95	0.96	7
	CG × *P*		5.91 ± 4	**1.05** ± 0.09	0.03	0.92	0.96	8.87
	CG	80	9.29 ± 2.01	**0.7** ± 0.03	< 0.005	0.95	0.96	9.94
	CG(1 - φ)		9.29 ± 2.01	**1.03** ± 0.05	< 0.005	0.95	0.96	10.7
	CG × *P*		13.48 ± 3.44	**0.95** ± 0.09	0.04	0.92	0.96	12.51
	CG	Fitted	8.46 ± 4.67	**0.77** ± 0.09	0.06	0.9	0.96	7.24
	CG(1 - φ)		-9.79 ± 6.06	**1.18** ± 0.12	0.05	0.91	0.96	4.79
	CG × *P*		-0.45 ± 3.08	**1.03** ± 0.06	0.01	0.95	0.96	3.48
Hyytiälä $\Delta^{18}O_{lw}$	CG	100	-0.58 ± 1.12	**0.98** ± 0.06	0.01	0.95	0.96	1.51
	CG(1 - φ)		-0.58 ± 1.12	**1.43** ± 0.08	0.01	0.95	0.96	5.26
	CG × *P*		2.32 ± 1.4	**1.33** ± 0.12	0.03	0.93	0.96	6.4
	CG	90	3.18 ± 0.86	**0.88** ± 0.05	0.01	0.95	0.96	1.68
	CG(1 - φ)		3.18 ± 0.86	**1.28** ± 0.07	0.01	0.95	0.96	6.57
	CG × *P*		4.61 ± 0.94	**1.27** ± 0.09	0.02	0.94	0.96	7.59
	CG	80	6.91 ± 0.63	**0.78** ± 0.04	0.01	0.95	0.96	4.12
	CG(1 - φ)		6.91 ± 0.63	**1.13** ± 0.06	0.01	0.95	0.96	8.3
	CG × *P*		7.28 ± 0.57	**1.2** ± 0.06	< 0.005	0.95	0.96	9.12
	CG	Fitted	5.46 ± 1.02	**0.99** ± 0.08	0.02	0.93	0.96	5.44
	CG(1 - φ)		1.74 ± 1.56	**1.13** ± 0.11	0.04	0.92	0.96	3.9
	CG × *P*		3.68 ± 1.24	**1.07** ± 0.09	0.03	0.93	0.96	4.88

[a]Significant relationship when slope is **bold** (p < .001).

Table 3. Linear mixed model fits between modelled and observed leaf water deuterium (Δ^2H_{lw}) and oxygen-18 ($\Delta^{18}O_{lw}$) enrichment in the studied large-scale dataset, with models using different intercellular relative humidity ($RH_{cellular}$ (%), Mechanism 1, n = 563).

		Intercept	Slope[a]	ICC	R^2(M)	R^2(C)	RMSE
Δ^2H_{lw}	100	-2.54 ± 2.43	**0.85** ± 0.03	0.3	0.61	0.91	18.83
	90	6.8 ± 2.18	**0.76** ± 0.02	0.29	0.62	0.91	15.58
	80	16.08 ± 1.95	**0.67** ± 0.02	0.28	0.63	0.91	13.68
	Fitted	10.52 ± 1.87	**0.8** ± 0.03	0.24	0.67	0.9	11.82
$\Delta^{18}O_{lw}$	100	1.02 ± 0.77	**0.83** ± 0.03	0.24	0.61	0.84	5.58
	90	4.08 ± 0.69	**0.74** ± 0.03	0.24	0.61	0.84	4.92
	80	7.12 ± 0.62	**0.66** ± 0.02	0.24	0.61	0.84	5.32
	Fitted	4.46 ± 0.64	**0.88** ± 0.03	0.21	0.66	0.86	5.06

[a]Significant relationship when slope is **bold** ($p < .001$).